Journal of Structural Geology 32 (2010) 1701–1711

Contents lists available at ScienceDirect

Journal of Structural Geology

journal homepage: www.elsevier.com/locate/jsg

The effect of the intermediate principal stress on fault formation and fault angle in siltstone

Bezalel Haimson [a,*], John W. Rudnicki [b]

[a] University of Wisconsin, Madison, WI 53706, USA
[b] Northwestern University, Evanston, IL 60208, USA

ARTICLE INFO

Article history:
Received 6 February 2009
Received in revised form
5 July 2009
Accepted 25 August 2009
Available online 11 September 2009

Keywords:
Bifurcation
Fault angle
Faulting
Siltstone
Mohr–Coulomb
Shear localization
Strength criterion
True triaxial test

ABSTRACT

We conducted true triaxial compression tests on specimens prepared from two siltstone core sections, one above and one below the Chelungpu Fault, Taiwan. For different constant σ_2 and σ_3 magnitudes, the maximum principal stress (σ_1) was raised until a post failure stage was reached, and a through-going fault had developed. Despite differences between the properties of the two cores, in all tests peak σ_1 increased as σ_2 was set at higher levels than σ_3, in contrast to Mohr–Coulomb condition predictions. The fault–normal vector was aligned with the σ_3 direction and made an angle (θ) with σ_1 direction. The angle θ, which corresponds to fault dip in case of normal faulting, increased monotonically with σ_2 for fixed σ_3, a variation that is also inconsistent with Mohr–Coulomb theory.

The results of shear band localization theory are used with fault angles observed for axisymmetric compression and deviatoric pure shear to infer properties of the inelastic constitutive behavior. These properties are significantly different for the two cores. Using them to predict θ for other deviatoric stress states yields good agreement with the observations for core II and acceptable agreement for core I. The results are used to predict the angle variation for constant mean normal stress (θ decreases as the deviatoric stress state varies from axisymmetric extension to axisymmetric compression) and at fixed deviatoric stress state (θ decreases monotonically with increasing mean normal stress).

1. Introduction

Laboratory experiments simulating compressive failure and faulting in rocks are typically conducted on cylindrical specimens subjected to constant lateral confining pressure and a rising axial load until brittle fracture occurs. These 'conventional triaxial tests' replicate only a special case of crustal condition, that in which two of the principal stresses are equal. Conventional triaxial tests on rocks were conducted as early as the turn of the last century (Von Kármán, 1911). They gained acceptance because of the relatively simple equipment, specimen preparation, and testing procedure. The ubiquity of conventional triaxial testing can also be traced to the assumption that the intermediate principal stress (σ_2) has a negligible effect on rock failure characteristics as expressed, for example, in the Mohr or Mohr–Coulomb failure criteria (Jaeger et al., 2007).

However, indications from the three major types of faulting encountered in the field, and results of numerous in situ stress measurements at depths reaching several kilometers (McGarr and Gay, 1978; Brace and Kohlstedt, 1980), point to a state of stress in the earth's crust that is fully three-dimensional ($\sigma_1 \neq \sigma_2 \neq \sigma_3$). Murrell (1963), Handin et al. (1967), and Mogi (1967) compared results of conventional triaxial compression tests with those of conventional triaxial extension and deduced that the differences in rock resistance to faulting between the two modes of loading were due to the different magnitudes of σ_2 applied. Inspired by this evidence, Mogi (1971) introduced a true triaxial testing machine in which rectangular prismatic specimens were subjected to three different principal stresses. He found that indeed σ_2 affects the stress level at which faulting occurs, and hence the rock strength criterion, as well as the angle at which the fault develops. Little follow-up on Mogi's seminal work took place until Haimson and co-workers carried out similar true triaxial tests in igneous rocks (Westerly granite, Haimson and Chang, 2000; Pohang rhyolite, Chang and Haimson, 2007); a metamorphic rock (KTB amphibolite, Chang and Haimson, 2000; Haimson and Chang, 2002) and a sedimentary rock (siltstone, Oku et al., 2007). They found that strength, deformability, and fault angle, were affected by σ_2 in all the tested rocks. An exception was found in tests of Long Valley (California)

* Corresponding author. Tel.: +1 608 262 2563.
E-mail address: bhaimson@wisc.edu (B. Haimson).

0191-8141/$ – see front matter © 2009 Elsevier Ltd. All rights reserved.
doi:10.1016/j.jsg.2009.08.017

ultra fine-grained hornfels and metapelite (Chang and Haimson, 2005), unusual rocks that appear to have no dilatancy, and develop no visible microcracks.

Independently, building upon the antecedents of Hadamard (1903), Mandel (1966), Thomas (1961) and Hill (1962), Rudnicki and Rice (1975) (also, Rice, 1976; Besuélle and Rudnicki, 2004) suggested a description of failure as a bifurcation from homogeneous (spatially uniform) deformation that predicted a strong dependence on σ_2 (via the deviatoric stress state). More specifically, Rudnicki and Rice (1975) established conditions for which a solution corresponding to concentrated deformation in a planar band was an alternative to continued homogeneous deformation. The appearance of this localized mode of deformation is often essentially coincident with "failure" by development of a through-going fault or fracture, but in other cases it may be the precursor to a more extended evolution of localized deformation that ultimately requires significant additional strain for failure. Analysis based on this approach yields a relation among constitutive parameters required for the onset of bifurcation and, hence, depends strongly on how the homogeneous deformation prior to bifurcation, especially the inelastic portion, is modeled.

The predictions of the failure stress by the bifurcation approach depend strongly on certain details of the constitutive behavior that are difficult to determine experimentally and, for various other reasons, are difficult to compare with experimental observations of failure (Besuélle and Rudnicki, 2004). However, the prediction for the fault angle is much less sensitive to these details and is more easily compared with observations in terms of the constitutive parameters for homogeneous deformation just prior to bifurcation. Rudnicki (2008a,b) has used and extended results from the bifurcation theory to interpret observations of failure plane inclinations in true triaxial tests of Westerly Granite (Haimson and Chang, 2000) and to infer aspects of the constitutive behavior.

In this paper we describe two series of true triaxial tests conducted on samples of siltstone taken from the hanging wall and the footwall of the Chelungpu fault, Taiwan. The tests reveal a clear dependency of strength and fault angle on the magnitude of σ_2. The results are compared with predictions based on shear localization theory incorporating a yield surface and plastic potential that depend on three stress invariants (rather than two, as in Rudnicki and Rice (1975)). Dependences of the yield surface and plastic potential on mean stress are inferred from the fault angles observed in axisymmetric compression and deviatoric pure shear. These dependences are used to compare the predicted fault angles with observations for other deviatoric stress states and to predict the variation that would be observed with mean stress for fixed deviatoric stress state and with deviatoric stress state for fixed mean stress.

2. Rocks tested

Rock specimens used in the true triaxial tests described here came from core recovered from the scientific hole A, near the northern end of the Chelungpu fault. The hole was drilled as part of the Taiwan Chelungpu Fault Drilling Project (TCDP). The project was undertaken to study the faulting mechanism behind the destructive Chi-Chi earthquake (1999; $M_w = 7.6$), characterized as a thrust motion across the North-South striking Chelungpu fault (Shin and Teng, 2001; Lin et al., 2003). Core made available to us came from short sections centered at the depth of 891 m (core I) and 1252 m (core II), straddling the active fault, which was intercepted at 1111 m. Core I is a siltstone belonging to the early Pleistocene Cholan Formation, which persists to a depth of 1013 m; core II is also a siltstone, belonging to the Pliocene Chinshui Formation, which prevails at depths of 1013–1313 m. Thus, core II is representative of the rock traversed by the active Chelungpu fault. Core I comes from a somewhat younger formation. As shown below, there are distinct differences in mineral content, as well as in mechanical behavior between the two siltstones. We cannot tell whether the differences are related to their juxtaposition with respect to the fault and its activity or, what appears more likely, the consequence of their different deposition ages.

The siltstone in core I contains 68% quartz, 19.5% clay, 9.5% feldspar, and 3% biotite; the siltstone in core II consists of 65% quartz, 25.5% clay, 7.5% feldspar, and 2% biotite. The only major difference is the amount of clay, and this may have a role in the disparity between the two core sections in some of their physical and mechanical properties (Table 1).

The 891 m siltstone is both stronger and stiffer in compression than the 1252 m core. Also notable is that core I rock has significantly larger grain size than core II. Although the siltstone is a sedimentary rock, no bedding planes were visible, and neither core showed signs of inhomogeneity. We examined the degree of anisotropy by running unconfined (uniaxial) compression tests in which cylindrical specimens (25.4 mm in diameter) were drilled out of the vertical core I at inclinations of 0°, 30°, 60°, and 90°. The compressive strengths in specimens from the four inclinations were all within 3% of the mean 79.4 MPa. Hence, we considered the siltstone to be basically isotropic with respect to strength. With respect to elastic modulus, the largest difference from the mean 13.7 GPa was less than 7%, a sign of a rather mild degree of anisotropy. These results enabled us to consider the siltstone practically isotropic.

3. Experiment setup and procedure

The apparatus used in our tests was a recently fabricated true triaxial testing machine (Haimson and Chang, 2000). As stated above, it had been successfully employed to characterize mechanical properties under the most general 3D state of stress of Westerly granite, KTB amphibolite, Long Valley hornfels and metapelite, and Pohang rhyolite. The true triaxial cell facilitates the application of three principal stresses to a rectangular prismatic specimen (size $19 \times 19 \times 38$ mm^3) by use of three independent servo-controlled units. The application of the maximum principal stress (σ_1) in the axial direction of the specimen and of the intermediate principal stress (σ_2) in one of the two lateral directions is carried out by use of two pairs of hydraulically driven pistons. The minimum principal stress (σ_3) is directly applied to the other pair of lateral faces by confining fluid pressure inside the cell. Details of the testing system, and its calibration, can be found in Haimson and Chang (2000).

In selected specimens strain gages for measuring strains in the direction of σ_1 and σ_2 were affixed to the faces subjected to σ_3 loading. Strain in the σ_3 direction was measured using a beryllium–copper strain-gaged beam mounted on one of the specimen σ_3 faces.

Table 1
Some physical and mechanical properties of core I and core II.

Property	Core I (891 m)	Core II (1252 m)
Mean grain size, μm	56 (200)	44 (200)
Dry density, kg/m^3	2594 (28)	2587 (28)
Effective porosity, %	6.9 (15)	6.1 (15)
Unconfined compressive strength (UCS), MPa	79.5 (2)	63.4 (2)
Young's modulus, GPa	13.7 (2)	9.2 (2)
Poisson's ratio	0.13 (2)	0.2 (2)
Brazilian tensile strength, MPa	5.4 (11)	4.2 (3)

Note: Numbers in parenthesis refer to the amount of measurements conducted.

The tests reported here were conducted under dry conditions. For that purpose the σ_3 faces, as well as the spaces between the edges of the anvils applying the other two loads were coated with a thin layer of polyurethane so that the confining fluid could not penetrate into the specimen. The scarcity of available core prevented us from testing saturated siltstone under pore pressure. However, that condition would have only affected the strength magnitudes, not the general mechanical behavior.

Testing procedure consisted of raising σ_1 at a constant strain rate of 8×10^{-6} s^{-1} while holding σ_2 and σ_3 at their preset magnitudes, until a post failure stage was reached, at which σ_1 had declined about 10% from its peak level. Upon unloading, tested specimens were sectioned along the σ_1–σ_3 plane in order to record fault attitude. In selected samples, sections were also prepared for SEM inspection.

4. Triaxial strength

4.1. Conventional triaxial strength

Conventional triaxial tests ($\sigma_2 = \sigma_3$) were first carried out in order to establish the Mohr strength criterion in terms of principal stresses, for later comparison with the true triaxial compressive strength ($\sigma_2 > \sigma_3$). The Mohr criterion was obtained by fitting a monotonically increasing power function to the experimental data (Fig. 1). In core I the best-fitting criterion is expressed by a power function:

$$\sigma_1 = 76.89 + 9.34\sigma_3^{0.80} (R = 0.997) \quad (1a)$$

In core II the Mohr criterion takes the form:

$$\sigma_1 = 73.23 + 6.36\sigma_3^{0.84} (R = 0.998) \quad (1b)$$

The fitting is excellent in both cases, with core II showing lower conventional triaxial strength. The experimental results in both cores can also be fitted by linear regression (Mohr–Coulomb criterion):

$$\sigma_1 = 94.9 + 3.6\sigma_3 (R = 0.992) \text{ for core I} \quad (2a)$$

$$\sigma_1 = 84.2 + 3.0\sigma_3 (R = 0.992) \text{ for core II} \quad (2b)$$

Again, core II proves to be weaker throughout the range of σ_3 (Fig. 2).

4.2. True triaxial strength

True triaxial tests were conducted for several constant magnitudes of σ_3. For a given σ_3, a series of tests were run, each at different σ_2 between $\sigma_2 = \sigma_3$ and σ_2 approaching peak σ_1. The results in terms of peak σ_1 versus σ_2 for the different preset σ_3 are plotted in Fig. 3a and b. The solid line in the plots represents the Mohr criterion determined from tests in which $\sigma_2 = \sigma_3$. Dashed curves show the trend of the true triaxial strength for each constant σ_3. The plots reveal a common characteristic of gradually increasing strength with the rise in σ_2 until a top level is reached, followed by a gradual decline, as predicted theoretically by Wiebols and Cook (1968) and confirmed by tests in other rocks by Mogi (1971), Haimson and Chang (2000), and Chang and Haimson (2000, 2007). The higher compressive strength when $\sigma_2 > \sigma_3$ as compared with that at $\sigma_2 = \sigma_3$ reveals the inadequacy of the Mohr (or Mohr–Coulomb) criterion to predict rock failure under the most general state of stress.

We attempted to determine the true triaxial strength criteria for siltstones by first employing Nadai's (1950) proposed relationship. He suggested a true triaxial strength criterion for brittle materials, such as rocks, in terms of the two stress invariants, octahedral shear stress (τ_{oct}) and octahedral normal stress, or mean stress (σ_{oct}). He related these invariants by a function (f) dependent on the rock material properties in the form of $\tau_{oct} = f(\sigma_{oct})$. Plotting all test results shown in Fig. 3 in the Nadai domain (Fig. 4) yields the following best-fit power function curves:

$$\tau_{oct} = 5.27\sigma_{oct}^{0.60} (R = 0.927) \text{ for core I} \quad (3a)$$

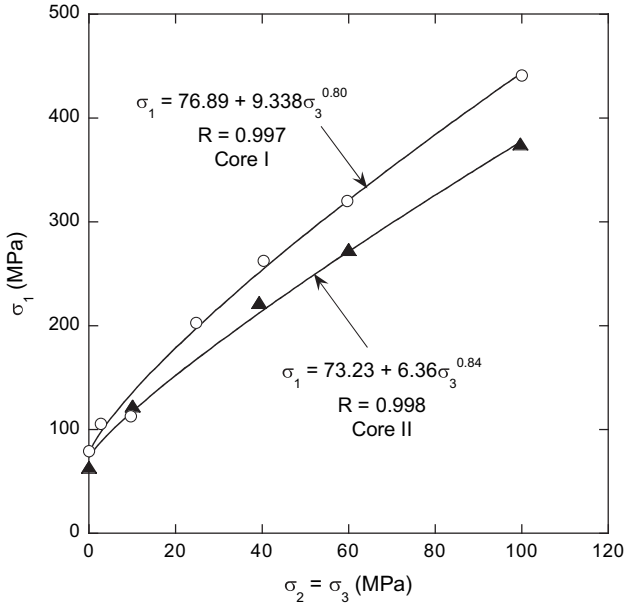

Fig. 1. Maximum compressive principal stress (σ_1) at failure as a function of the least principal stress (σ_3) under conventional triaxial stress condition ($\sigma_2 = \sigma_3$), and the best-fitting power function strength criterion (Mohr) for each of the two siltstone cores.

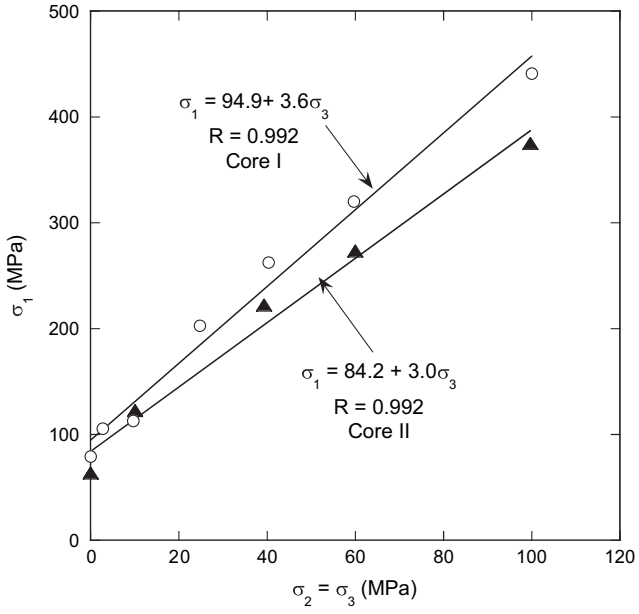

Fig. 2. Maximum compressive principal stress (σ_1) at failure as a function of the least principal stress (σ_3) under conventional triaxial stress condition ($\sigma_2 = \sigma_3$), and the best-fitting linear strength criterion (Mohr–Coulomb) for each of the two siltstone cores.

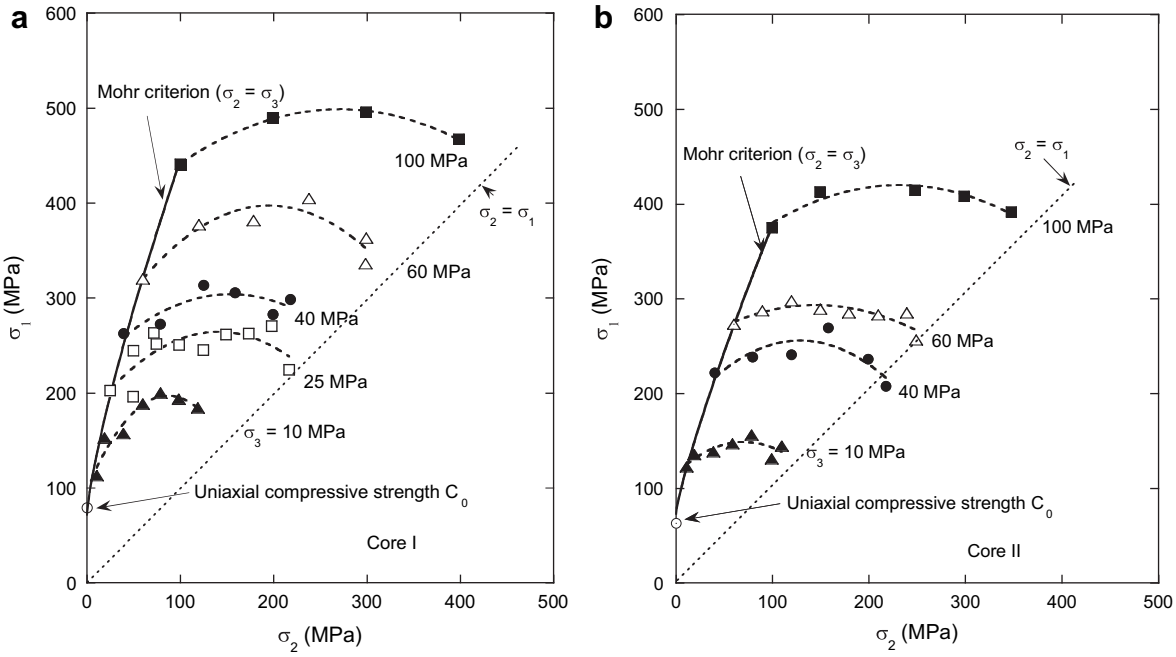

Fig. 3. Variation of peak compressive stress σ_1 as a function of σ_2 for different constant values of σ_3 (a) in the core I and (b) in core II.

$$\tau_{oct} = 5.10\sigma_{oct}^{0.58} (R = 0.915) \text{ for core II} \quad (3b)$$

where

$$\tau_{oct} = \left\{ \left[(\sigma_1 - \sigma_2)^2 + (\sigma_2 - \sigma_3)^2 + (\sigma_3 - \sigma_1)^2 \right]^{1/2} \right\} \Big/ 3 \quad (4)$$

and

$$\sigma_{oct} = (\sigma_1 + \sigma_2 + \sigma_3)/3 \quad (5)$$

The Nadai criterion appears to fit the data reasonably well, albeit with considerable scatter.

Mogi (1971) adjusted the Nadai criterion to correspond with the mode of compressive failure in brittle rock, which does not occur over the entire volume (as expressed by Eqs. (3)), but is restricted to faulting along a plane aligned with the σ_2 direction. For this reason he replaced σ_{oct} with the mean stress acting on the plane of failure ($\sigma_{m,2}$). All data points in Fig. 3 are well-fitted by a power function in Mogi's domain (Fig. 5):

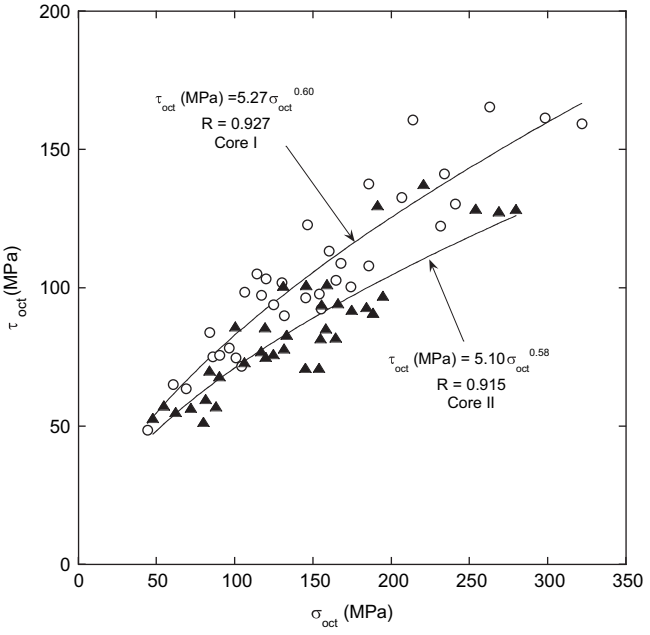

Fig. 4. A true triaxial strength criterion for the siltstone (cores I and II), based on all the experimental results shown in Fig. 3, in the Nadai (1950) domain of τ_{oct} versus σ_{oct}.

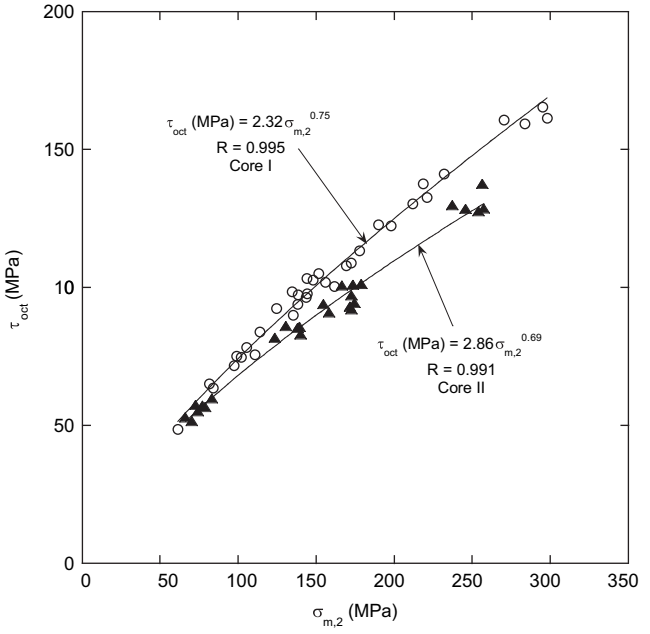

Fig. 5. A true triaxial strength criterion for the siltstone (cores I and II), based on all the experimental results shown in Fig. 3, in the Mogi (1971) domain of τ_{oct} versus $\sigma_{m,2}$.

$$\tau_{oct} = 2.32\sigma_{m,2}^{0.75} (R = 0.995) \text{ for core I} \quad (6a)$$

$$\tau_{oct} = 2.86\sigma_{m,2}^{0.69} (R = 0.991) \text{ for core II} \quad (6b)$$

where

$$\sigma_{m,2} = (\sigma_1 + \sigma_3)/2 \quad (7)$$

Comparison between Figs. 4 and 5 makes it clear that Mogi's relationship (Eqs. (6)) better represents the true triaxial strength criteria for both cores. A physical interpretation of Eqs. (6) is that brittle failure, or faulting, occurs when the distortional strain energy reaches a critical value that increases monotonically with the mean normal stress on the failure plane.

5. Fault angle

Failure in true triaxial tests took the form of single or conjugate through-going faulting. The fault–normal direction and the angle (θ) between it and σ_1 were carefully measured at the conclusion of each test. Under conventional triaxial stresses fault–normal direction was random since $\sigma_2 = \sigma_3$. Conventional triaxial strength data appear to be fitted well by the Mohr–Coulomb criterion (Fig. 2). The linear relationship represented by this criterion enables the computation of the unique angle of internal friction ϕ:

$$\phi = 34.6^\circ \text{ for core I} \quad (8a)$$

$$\phi = 30.3^\circ \text{ for core II} \quad (8b)$$

Subsequently, the theoretical fault angle θ is also unique, regardless of σ_2 or σ_3 magnitudes:

$$\theta = 45^\circ + 34.6/2 = 62.3^\circ \text{ for core I} \quad (9a)$$

$$\theta = 45^\circ + 30.3/2 = 60.2^\circ \text{ for core II} \quad (9b)$$

However, the fault angles measured in tested specimens that have been subjected to conventional triaxial stress conditions show a gradual decrease from 73° to 59° in core I, and from 76° to 52° in core II, as $\sigma_2 = \sigma_3$ increases from 10 MPa to 100 MPa (Fig. 6). A similar trend of fault angle decrease with confining pressure increase has been documented in other rocks, such as Fontainebleau sandstone (Haied et al., 2000), Westerly granite (Haimson and Chang, 2000), and KTB amphibolite (Chang and Haimson, 2000). This variation of the fault angle with lateral stress contradicts the prediction based on the Mohr–Coulomb criterion (Eqs. (9)).

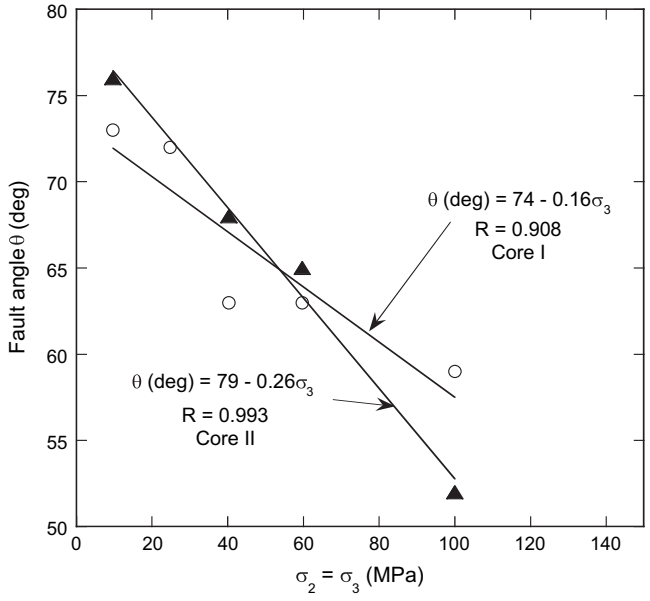

Fig. 6. Fault angle (θ) variation with $\sigma_2 = \sigma_3$ under conventional triaxial stress conditions (cores I and II).

In true triaxial tests the trend in both cores is for the fault angle to increase with σ_2 for constant σ_3. The total increase is limited to about 10° in the two siltstones, less than in the Westerly granite (Haimson and Chang, 2000) or the KTB amphibolite (Chang and Haimson, 2000), but still significant. Fig. 7a and b shows the results of all measured fault angles. The increase in fault angle with σ_2 for constant σ_3 cannot be explained by Mohr theory (Eqs. (1) or (2)), which neglects the effect of σ_2 on rock failure. Using the power function strength criterion (Mohr) in Fig. 3 would introduce a dependence of the fault angle on σ_2 but not on σ_3.

6. Fault angle prediction from bifurcation theory

Rudnicki and Rice (1975) gave a prediction for the fault angle for the most general form of a rate-independent, elastically isotropic–plastic constitutive relation with a smooth yield surface (the surface that forms the boundary of the stress states that cause only elastic deformation) and plastic potential (which gives the direction of the inelastic strain increments in stress space) that depend only on two of the three stress invariants. This form included the possibility of dependence of the yield stress in shear on mean stress (either positive, as on a frictional yield surface or negative, as on a yield surface "cap") and inelastic volume change (either compaction or dilatancy). Rudnicki and Olsson (1998) gave a more convenient rearrangement of the Rudnicki and Rice result. This expression also incorporates a correction (Perrin and Leblond, 1993; also, noted by Ottosen and Runesson, 1991) for the limiting cases in which the band is predicted to be perpendicular to the most compressive stress ("compaction band") or the least compressive stress ("dilation band") rather to the intermediate principal stress, which is the most common case.

Ottosen and Runesson (1991) derived an expression for the predicted fault angle for a yield surface and plastic potential that depended on all three stress invariants. Rudnicki (2008a) noted that the prediction could be obtained by replacement of certain quantities in the original Rudnicki and Rice (1975) expression. This result is explained in more detail in Rudnicki (2008b) and summarized here.

From the experimental point of view, it is natural to express results in terms of the principal stresses, since these are the quantities applied or measured. Conceptually, however, it is more natural to use the stress invariants. For an isotropic material these two representations are completely equivalent. For example, the Nadai criterion (Eq. (3)) can be expressed in terms of two invariants whereas the Mohr–Coulomb or Mogi criterion (Eq. (6)) requires three. Using the stress invariants has the advantage that they are independent of the particular choice of axes and, in applications; this avoids the necessity of determining principal stress directions at each point. More importantly, from a physical point of view, we expect that the shear (deviatoric) stress and mean (hydrostatic stress) have different effects on rock behavior. These contributions are clearly identified by the invariants, whereas changing a particular principal stress changes both the deviatoric and mean stresses.

The theory is based on forms for the yield surface and the plastic potential surface that depend on all three stress invariants. The invariants used here are chosen as follows: The von Mises equivalent

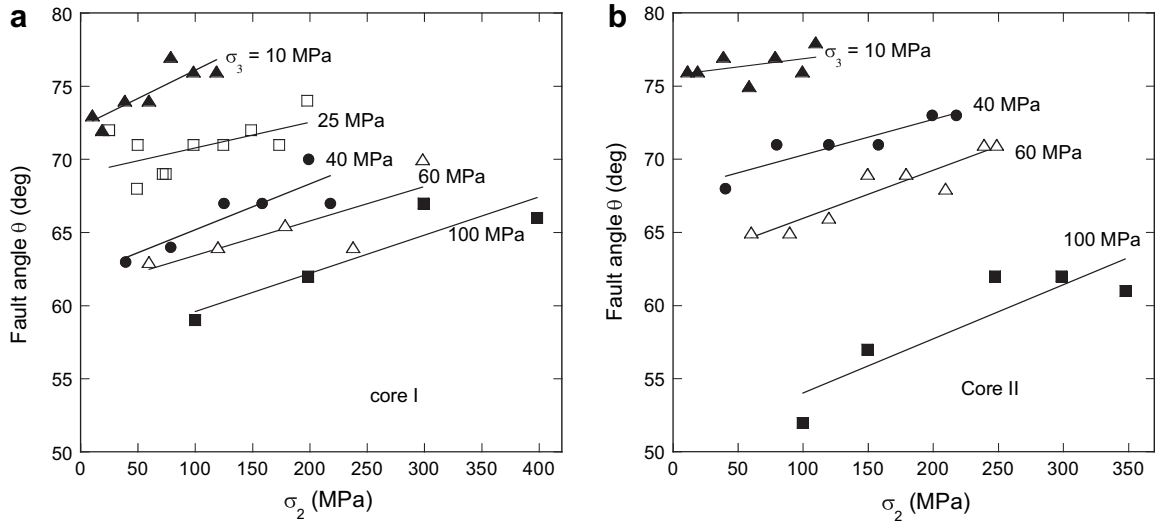

Fig. 7. Measured fault angle (θ) variation with σ_2 for different magnitudes of constant σ_3 (a) for core I, and (b) for core II.

stress τ which is equal to $\sqrt{3/2}\tau_{oct}$ (Eq. (4)), σ_{oct} (Eq. (5)), and the Lode angle θ_L. The Lode angle is defined as $3\theta_L = \arcsin(\sqrt{27}J_3/2\tau^3)$ where $J_3 = \det(s_{ij})$ is the third invariant of the deviatoric stress. (The difference in sign from Rudnicki (2008a,b) occurs because stresses are taken as positive in compression here). In the space of principal stresses, θ_L is the angle in planes that are normal to the hydrostat $\sigma_1{=}\sigma_2{=}\sigma_3$ and for which σ_{oct} is constant. The angle θ_L is zero for deviatoric pure shear ($\sigma_2 = (\sigma_1 + \sigma_3)/2$), and varies between $-\pi/6(-30^\circ)$ for axisymmetric extension ($\sigma_1 = \sigma_2$) and $\pi/6(+30^\circ)$ for axisymmetric compression ($\sigma_3 = \sigma_2$). For an isotropic material the remaining five sectors (of 60°) are given by symmetry.

In terms of the three invariants just defined, the yield condition and plastic potential are given by equations of the form $F(\tau, \sigma_{oct}, \theta_L) = 0$ and $G(\tau, \sigma_{oct}, \theta_L) = 0$, respectively. Both will generally be functions of additional parameters that keep track of the history of inelastic deformation and are not displayed here. Values of constitutive parameters will evolve with inelastic deformation but those that enter the fault angle predictions are those just prior to bifurcation.

The direction of the inelastic strain increments (in stress space) coincides with the normal to the plastic potential surface $P_{ij} = \partial G/\partial\sigma_{ij}$. The normal to the yield surface is $Q_{ij} = \partial F/\partial\sigma_{ij}$ and is not in the same direction as the normal to the plastic potential. For geomaterials it is typically the case that $P_{kk} \neq Q_{kk}$ or that $F_\sigma \neq G_\sigma$ (where the subscript denotes partial differentiation with respect to σ_{oct}). Geometrically, in a space where the principal stresses are taken as axes, the normal to the yield surface differs from the direction of inelastic strain increments in planes that contain the hydrostatic axis $\sigma_1 = \sigma_2 = \sigma_3$. Physically, this means that the ratio of increments of τ to σ_{oct} does not equal the ratio of the increments of inelastic volume strain (positive in dilation) to equivalent inelastic shear strain, defined by $d\gamma^p = (2de^p_{ij}\, de^p_{ij})^{1/2}$ where de^p_{ij} is the deviatoric portion of the inelastic strain increment. The direction of inelastic strain increments is taken to be normal to the projection of the yield surface in deviatoric planes (planes normal to the hydrostatic axis) because there are neither observational evidence nor physical grounds indicating otherwise. As a result, the deviatoric parts of the normals to the yield surface and plastic potential are identical, $P'_{ij} = Q'_{ij}$, where the prime denotes the deviatoric part, and $G_\tau = F_\tau$ and $G_{\theta_L} = F_{\theta_L}$.

With these definitions and assumptions the fault angle is given by

$$\theta = (\pi/4) + (1/2)\arcsin\alpha \tag{10}$$

where

$$\alpha = \frac{(1/3)(1+\nu)(P_{kk}+Q_{kk}) + Q'_2(1-2\nu)}{\sqrt{4\left(Q'_{ij}Q'_{ij}\right) - 3\left(Q'_2\right)^2}} \tag{11}$$

ν is Poisson's ratio and Q'_2 is the intermediate principal deviatoric value of Q_{ij} Eq. (11) can be expressed in terms of derivatives of the yield function and plastic potential as

$$\alpha = \frac{-(1+\nu)\cos\psi(F_\sigma + G_\sigma)/F_\tau + (1-2\nu)\sin(\psi+\theta_L)/\sqrt{3}}{\cos(\psi+\theta_L)} \tag{12}$$

by using the following relations:

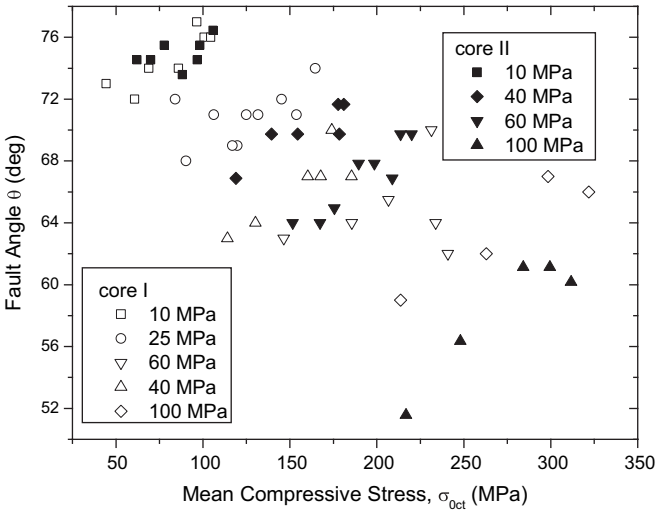

Fig. 8. Measured fault angle (θ) variation with σ_{oct} for different magnitudes of constant σ_3 (different symbols) for core I (open) and core II (solid).

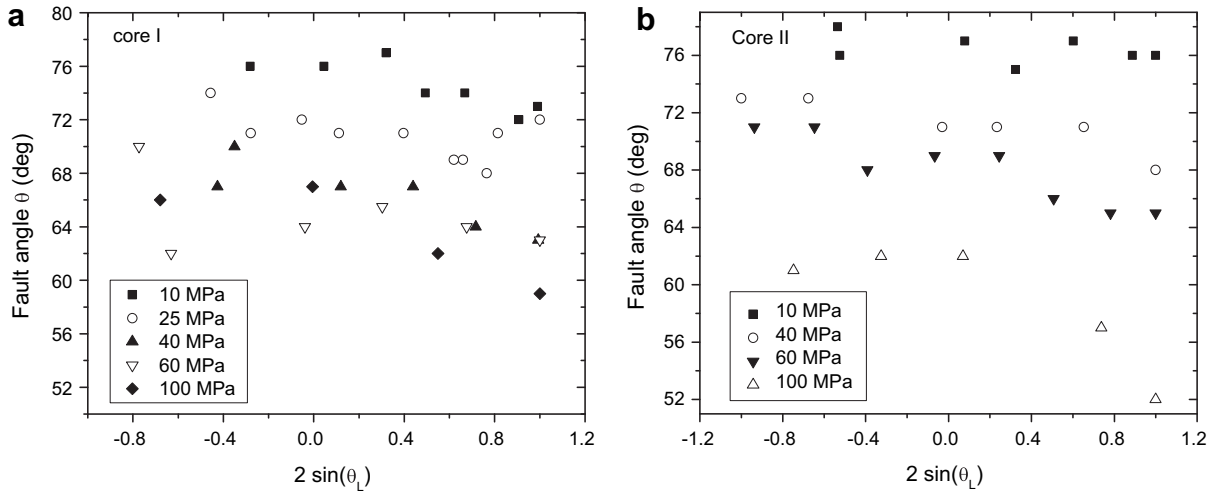

Fig. 9. Measured fault angle (θ) variation with deviatoric stress state, from axisymmetric extension (-1, left) to axisymmetric compression ($+1$, right) for different magnitudes of constant σ_3 (different symbols) for core I (a) and core II (b).

$$P_{kk} = 3G_\sigma, \quad Q_{kk} = 3F_\sigma, \quad \tan\psi = \frac{F_{\theta_L}/\tau}{F_\tau}, \quad 2Q'_{ij}Q'_{ij} = \left(F_{\theta_L}/\tau\right)^2 + (F_\tau)^2 \tag{13}$$

and

$$\frac{Q'_2}{\sqrt{Q'_{ij}Q'_{ij}/2}} = -\frac{2}{\sqrt{3}}\sin(\psi + \theta_L) \tag{14}$$

Eq. (12) reduces to the Rudnicki and Olsson (1998) form of the Rudnicki and Rice (1975) expression by setting $\psi = 0$, noting that $F_\sigma/F_\tau = -3\mu$, $G_\sigma/F_\tau = -3\beta$ and $\sin\theta_L = (\sqrt{3}/2)N$, where $N = -s_2/\tau$ is the deviatoric stress state parameter used by Rudnicki and Rice (1975) (again, the minus sign occurs here because stresses are positive in compression).

To use Eq. (12) to make predictions for comparison with data it is necessary to adopt a specific form for the yield condition. Rudnicki (2008a) showed that although limited agreement with data on Westerly granite could be achieved with a two invariant constitutive model (no dependence on θ_L), better agreement was possible with a yield condition of the following form:

$$-\sqrt{\frac{4}{27}}\,A\sin(3\theta_L)\left(\frac{\tau}{\tau_0}\right)^3 + \left(\frac{\tau}{\tau_0}\right)^2 - 1 = 0 \tag{15}$$

where $0 \le A \le 1$. If $A = 0$, then the shape of the yield surface in the deviatoric plane reduces to a circle with the radius determined by $\tau_0(\sigma_{oct})$. When $A = 1$, the shape reduces to a triangular Rankine type model, in which yield is determined by a critical value of the least compressive stress. Rudnicki (2008b) has discussed how assuming that τ_0 is proportional to σ_{oct} and particular choices for the constant of proportionality and A duplicate the forms suggested by Lade and Duncan (1975) and Matsuoka and Nakai (1974) (also described in Borja et al., 2003).

In general, A, in addition to τ_0, could depend on the octahedral normal stress, σ_{oct}, but we use a constant value of 0.7 here. Limited experimentation indicated no strong dependence on A (as long as it was not near its limits) but we made no attempt to optimize the choice to agree with the data.

Because the first term in Eq. (15) vanishes for $\theta_L = 0$, $\tau_0(\sigma_{oct})$ gives the mean stress dependence of the yield stress in deviatoric pure shear ($\sigma_2 = (\sigma_1 + \sigma_3)/2$). Evaluating the third of Eqs. (13) for Eq. (15) yields an expression for $\tan\psi$ and the ratio $F_\sigma/\tau F_\tau$ is given by

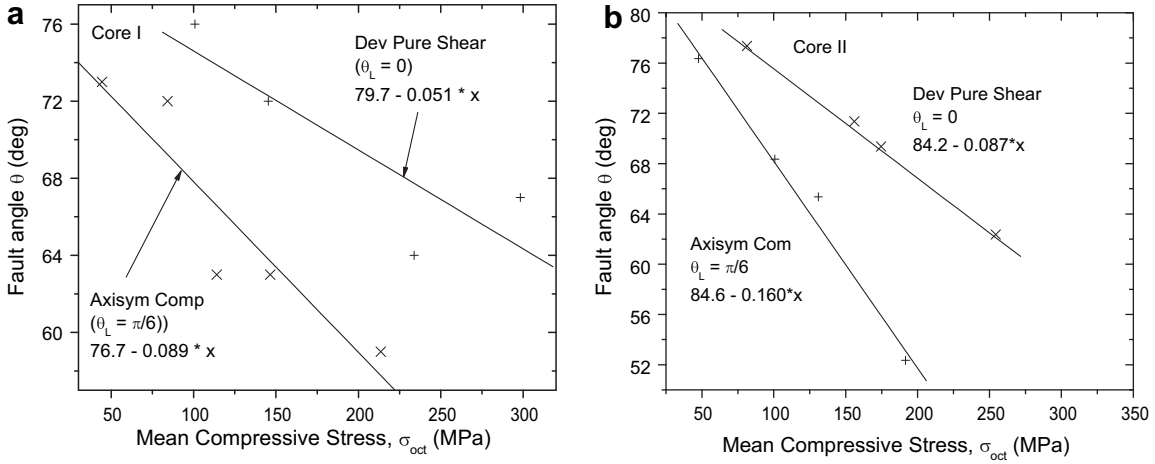

Fig. 10. Fault angle (θ) variation with σ_{oct} for axisymmetric compression ($\theta_L = \pi/6$) and deviatoric pure shear ($\theta_L = 0$) for core I (a) and core II (b).

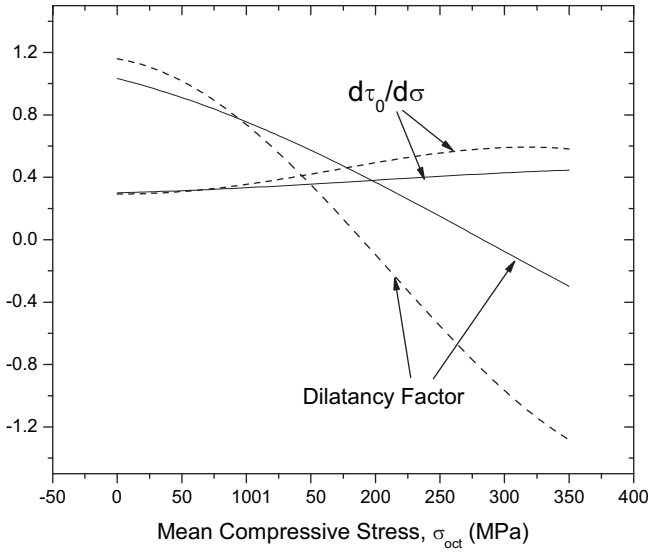

Fig. 11. Solutions for $d\tau_0/d\sigma$, Eq. (16), and the dilatancy factor β, Eq. (17), as functions of σ_{oct} based on linear fits in Fig. 10. Solid lines show results for core I and dashed for core II.

$$\frac{F_\sigma}{\tau F_\tau} = \frac{\tau}{\tau_0}\frac{d\tau_0(\sigma_{oct})}{d(\sigma_{oct})} \tag{16}$$

because $\tau = \tau_0$ for pure shear $\theta_L = 0$, Eq. (16) gives a friction coefficient (which will be different for other deviatoric stress states, e.g., axisymmetric compression or extension). A similar ratio could be inferred from the data shown in Fig. 4, but would pertain to the slope of the failure surface rather than to the yield function. The failure surface can be quite different from yield surface (even evaluated at failure) (see, e.g., Holcomb and Rudnicki (2001) or Besuélle and Rudnicki (2004)).

A consequence of the requirement that normality be satisfied in the deviatoric plane (see end of paragraph preceding Eq. (10)) is that the yield function and plastic potential can differ only by a function of $\sigma = \sigma_{oct}$ that we denote by $H(\sigma)$. A dilatancy factor β, the ratio of the inelastic increment of volume strain to inelastic increment of shear strain (defined earlier) is given by

$$\beta = \frac{3}{2}\frac{1}{\sqrt{1+A^2/3}}\left\{2\frac{d\tau_0}{d\sigma_{oct}} + \tau_0 H'(\sigma_{oct})\right\} \tag{17}$$

As for Eq. (16), this expression applies for pure shear and would be slightly different for other deviatoric stress states.

7. Application to TCDP data

Because the yield surface and predictions for the band angle are expressed in terms of invariants of the stress rather than the principal stresses themselves, we plot the observed fault angle versus the mean compressive stress σ_{oct} (in Fig. 8) and the Lode angle θ_L (in Fig. 9). If both the mean stress and Lode angle are known then the value of τ is determined by the yield condition. In Fig. 8, both core I and core II show an approximately linear increase in fault angle with σ_{oct} for fixed values of least compressive stress, but an overall decrease in band angle with increasing mean stress. Figs. 9a (core I) and Fig. 9b (core II) show the fault dip angle plotted against 2 sin θ_L which varies from -1 on the left for axisymmetric extension, through 0 for deviatoric pure shear, to $+1$ for axisymmetric compression on the right. Data from both cores appear to show a slightly decreasing dip angle for increasing Lode angle, but this is more evident for core II.

As already noted, the tests were conducted for fixed values of the least compressive stress. Consequently, neither σ_{oct} nor θ_L is constant in the tests and it is difficult to infer the dependence on either from Figs. 8 and 9. Nevertheless, within both data sets are several tests for axisymmetric compression ($\sigma_2 = \sigma_3$, $\theta_L = \pi/6$) and near pure shear ($\sigma_2 = (\sigma_1 + \sigma_3)/2$, $\theta_L = 0$). Here "near" means $|2 \sin \theta_L| \leq 0.05$ for core I and 0.08 for core II. Fig. 10a (core I) and Fig. 10b (core II) show the fault angles for axisymmetric compression and pure shear against σ_{oct} and linear fits through the data for each deviatoric stress state. All the slopes are negative, but the magnitudes are greater for core I than for core II. For each core the magnitude of the slope is larger for axisymmetric compression than for deviatoric pure shear, by nearly a factor of 2 for core II.

Substituting the linear relations shown in Fig. 10 into Eq. (12), using Eq. (15), and evaluating for pure shear ($\theta_L = 0$) and axisymmetric compression ($\theta_L = \pi/6$) yields two linear equations for the unknown functions of σ: $d\tau_0/d\sigma$ (Eq. (16)) and $H'(\sigma)$ (Eq. (17)). Fig. 11 shows the solutions for the two data sets. For both the variation is greater for core II than for core I.

Values of $d\tau_0/d\sigma$, which has the interpretation of a friction coefficient, are reasonable, though, perhaps, on the low side, for both core I and core II. The slight increase with mean stress is, however, surprising as friction coefficient nearly always decreases with increasing mean stress. For comparison, a friction coefficient

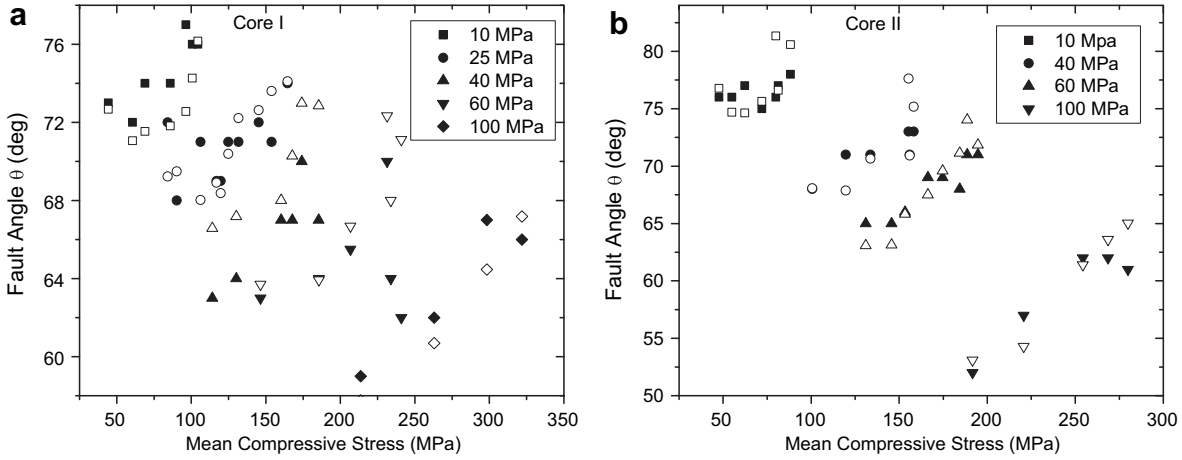

Fig. 12. Comparison of predicted (open symbols) with observed (filled symbols) fault angles plotted against mean compressive stress (σ_{oct}) for core I (a) and core II (b).

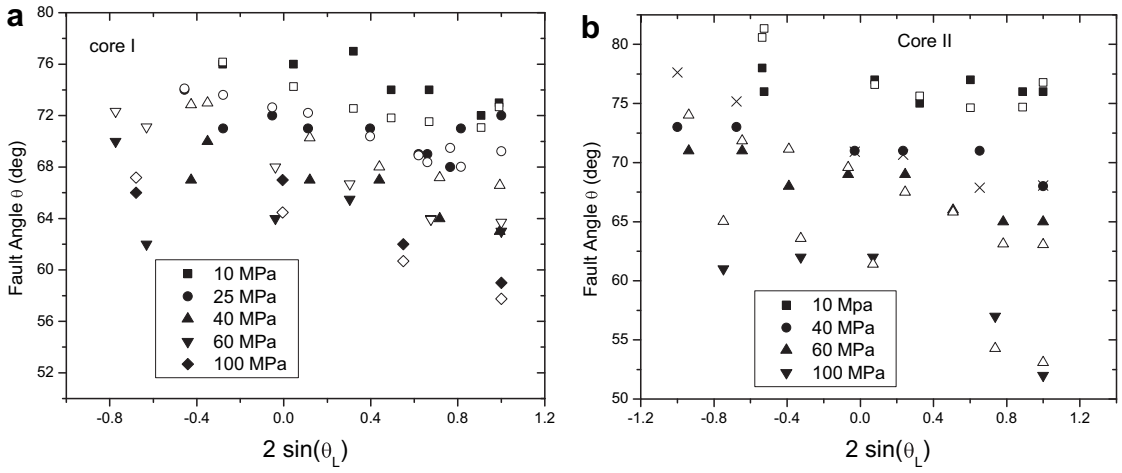

Fig. 13. Comparison of predicted (open symbols) with observed (filled symbols) fault angles plotted against deviatoric stress state ($2 \sin \theta_L$) for core I (a) and core II (b).

calculated as the slope of the curve for core I in Fig. 4 decreases from 0.66 at 50 MPa to 0.30 at 350 MPa. That for core II decreases from 0.57 to 0.25 over the same range of compressive stress. The increase shown in Fig. 11 is, however, not large and given the idealizations of the model and variation in the data, it has questionable significance.

The values for the dilatancy factor decrease substantially with mean stress. This is as expected but the magnitude of the values at low and high confining stresses are surprisingly large. The values at low mean stress are around 1 and indicate very strong dilatancy. Values for core I decrease to a small negative value, about −0.3 at the highest mean stress. Although a decrease of dilatancy with mean stress is reasonable, it is less likely that compaction would occur, even at the highest mean stress, given the relatively low porosity and the history of significant shear. The very strong compaction predicted for core II at high mean stress is not realistic.

Some aspects of the functions plotted in Fig. 11 are in accord with expected behavior, but it seems difficult to assign them more than qualitative significance. It is, however, interesting that the behavior inferred for the two cores is significantly different. Despite the questionable aspects of the plots in Fig. 11, they are based on the observed decrease in band angle with mean stress for pure shear and axisymmetric compression shown in Fig. 10 and will, of course, reproduce this behavior. This is a significant improvement over constitutive models based on only two of the stress invariants. In addition, the predicted band angle (see Eq. (12)) depends primarily on the sum of the two functions. For this reason, it seems that the slight increase with mean stress predicted for the friction coefficient is compensated by an excessive decrease in the dilatancy factor. At this point, it is unclear what improvement might lead to a more reasonable division.

The functions of mean stress shown in Fig. 11 are then re-substituted into Eq. (12) using Eq. (15) and used to evaluate the predicted band angles for all the Lode angles in the measured data. Fig. 12a (core I) and Fig. 12b (core II) show the fault angle data and predictions plotted against the mean compressive stress (with the open symbols showing the predictions). Clearly, the agreement is much better for core II (correlation 95%) than for core I (correlation 80%). Fig. 13 plots the same data against the Lode angle parameter ($2 \sin \theta_L$). Not surprisingly, for both the agreement is better for positive values since the mean stress variation used the data for pure shear $\theta_L = 0$ and axisymmetric compression ($\theta_L = \pi/6$).

Figs. 14 and 15 show the predicted fault angles if tests were conducted at fixed values of mean stress or of Lode angle θ_L. Fig. 14 plots the fault angle against mean compressive stress for five values of θ_L corresponding to fixed deviatoric stress states. As expected,

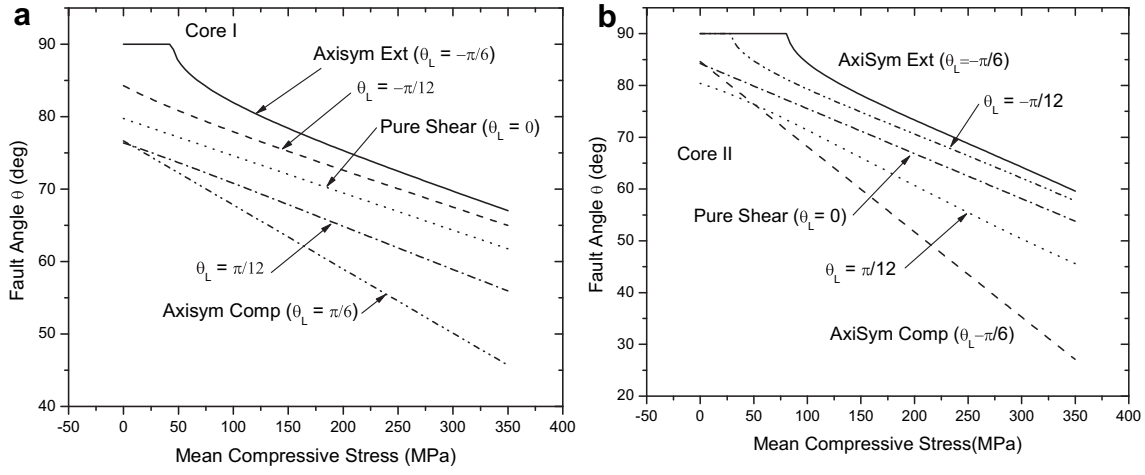

Fig. 14. Predicted variation of the fault angle against mean compressive stress (σ_{oct}) for constant deviatoric stress states ($2 \sin \theta_L$) for core I (a) and core II (b).

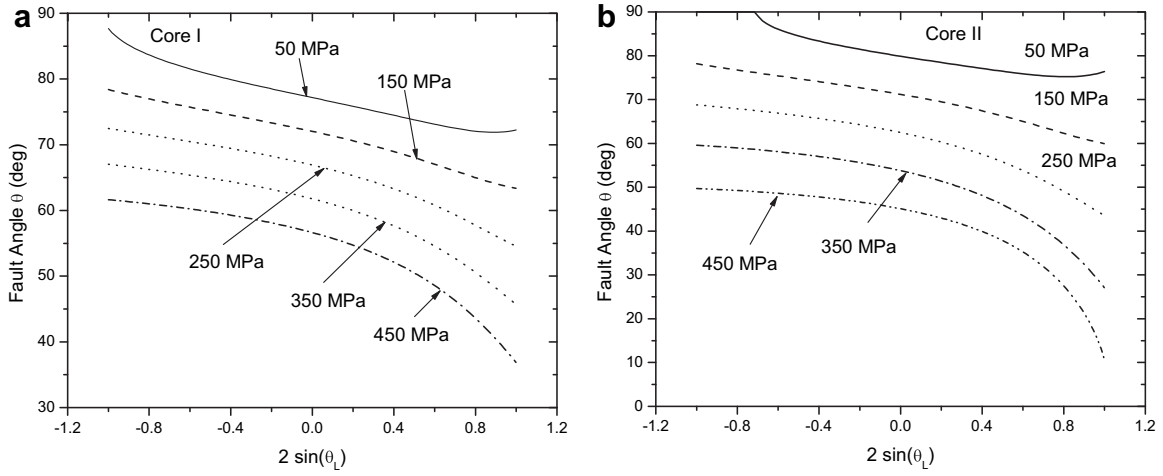

Fig. 15. Predicted variation of the fault angle against deviatoric stress state ($2 \sin \theta_L$) at five constant values of σ_{oct} for core I (a) and core II (b).

the fault angles decrease with increasing mean stress. The straight lines for axisymmetric compression and pure shear reflect the use of these data in the fitting. For both cores dilation bands (perpendicular to least compressive stress; extension fractures) are predicted for axisymmetric extension at the lowest mean normal stresses, though stress states corresponding to $\theta < \theta_L$ are not well populated by the data. For axisymmetric compression at the highest mean stresses the angles extend down to slightly less than 50° for core I. For core II they extend down to 30°, suggesting the possibility of compaction band formation at mean stresses somewhat higher than achieved in the tests. This prediction is also consistent with the strong compaction inferred for core II at higher mean stresses (Fig. 11b).

Fig. 15 plots the fault angle against the deviatoric stress state parameter for five constant values of the mean compressive stress. The band angle decreases as the deviatoric stress state varies from axisymmetric extension (left side) to axisymmetric compression (right side). This trend is consistent with the predictions of the simpler constitutive relation used by Rudnicki and Rice (1975) although the decrease here is not so large. Because the fault angle also decreases with mean compressive stress, the variations with mean stress and deviatoric stress states can offset or augment each other. The results for core II predict a dilation band for the lowest mean stress. Although neither result shows a compaction band, the fault angle does decrease rapidly approaching axisymmetric compression for the highest mean stress values shown. Rudnicki (2004) has suggested this rapid decrease as a possible reason for the infrequent observation of dip angles in this range.

8. Conclusions

True triaxial tests on two siltstone cores from the TCDP hole A reveal that the intermediate principal stress is a significant contributor to their compressive strength, and bring into question the suitability of the Mohr and Mohr–Coulomb strength criteria, which neglect the effect of σ_2. Rather, strength criteria in terms of the invariants octahedral shear stress and the 2-D mean stress in the σ_1–σ_3 plane fit well the experimental data.

The angle of the fault created upon brittle fracture, is also strongly affected by σ_2. It is found that the angle rises with σ_2 for constant σ_3, further questioning the adequacy of the Mohr-type criteria, which predict a fault angle independent of σ_2.

The variation of the fault angle with mean compressive stress and deviatoric stress state is modeled using localization theory with a three invariant form for the yield function and plastic potential. Calibration of the results using subsets of the data for deviatoric pure shear and axisymmetric compression yields two inelastic properties that are functions of the mean stress. Incorporating these inferred functions, the predictions agree well with the entire data set for core II and acceptably with that for core I. The results are then used to predict the variation for the band angle for true triaxial tests conducted at constant mean stress and fixed deviatoric stress state. The fault angle at constant mean normal stress is predicted to decrease as the deviatoric stress state varies from axisymmetric extension to axisymmetric compression. The fault angle at fixed deviatoric stress state is predicted to decrease monotonically with increasing mean normal stress.

Although the inferred inelastic constitutive functions are reasonable, there is no independent verification of their form. Nor are there true triaxial tests available at constant mean stresses or deviatoric stress state. Nevertheless the variation of observed fault angle is clearly not well-described by the simple Mohr–Coulomb type theory. Comparison with the more elaborate theory, despite the uncertainties involved, yields predictions that could be evaluated by further testing and offers insight into the inelastic constitutive behavior of the rock and its relation to failure.

Acknowledgements

Partial financial support for JWR was provided by the US Dept. of Energy, Office of Science, Basic Energy Sciences, Geosciences Program through grant DE-FG02-93ER14344/A016 to Northwestern University. Partial financial support for BH was provided by NSF grant EAR-0346141. Thanks are extended to H. Oku for carrying out the laboratory experiments and to Florent Gimbert for many helpful discussions about three invariant constitutive relations. Core from the TCDP was obtained courtesy of Professor Sheng-Rong Song, National Taiwan University. The authors also thank Philip Benson and an anonymous reviewer for comments that improved the paper.

References

Besuélle, P., Rudnicki, J.W., 2004. Localization: shear bands and compaction bands. In: Guéguen, Y., Boutéca, M. (Eds.), Mechanics of Fluid Saturated Rocks. International Geophysics Series, 89. Academic Press, London, pp. 219–321.

Borja, R.I., Sama, K.M., Sanz, P.F., 2003. On the numerical integration of three-invariant elastoplastic constitutive models. Computer Methods in Applied Mechanics and Engineering 192, 1227–1258.

Brace, W.F., Kohlstedt, D.L., 1980. Limits on lithospheric stress imposed by laboratory experiments. Journal of Geophysical Research 85 (B11), 6248–6252.
Chang, C., Haimson, B.C., 2000. True triaxial strength and deformability of the KTB deep hole amphibolite. Journal of Geophysical Research 105, 18999–19014.
Chang, C., Haimson, B.C., 2005. Nondilatant deformation and failure mechanism in two Long Valley Caldera rocks under true triaxial compression. International Journal Rock Mechanics and Mining Sciences 42, 402–414.
Chang, C., Haimson, B., 2007. Effect of fluid pressure on rock compressive failure in a nearly impermeable crystalline rock: implication on mechanism of borehole breakouts. Engineering Geology 89, 230–242.
Hadamard, J., 1903. Leçons sur la Propagation de Ondes et Les Eqs. de L'Hydrodynamique, Paris.
Haied, A., Kondo, D., Henry, J.P., 2000. Strain localization in Fontainebleau sandstone. Mechanics of Cohesive–Frictional Materials 5, 239–253.
Haimson, B., Chang, C., 2000. A new true triaxial cell for testing mechanical properties of rock, and its use to determine rock strength and deformability of Westerly granite. International Journal of Rock Mechanics and Mining Sciences 17, 285–296.
Haimson, B., Chang, C., 2002. True triaxial strength of the KTB amphibolite under borehole wall conditions and its use to estimate the maximum horizontal in situ stress. Journal of Geophysical Research 107 (B10) ETG 15-1 to 14.
Handin, J., Heard, H.C., Magouirk, J.N., 1967. Effect of the intermediate principal stress on the failure of limestone, dolomite, and glass at different temperature and strain rate. Journal of Geophysical Research 72, 611–640.
Hill, R., 1962. Acceleration waves in solids. Journal of the Mechanics and Physics of Solids 19, 1–16.
Holcomb, D.J., Rudnicki, J.W., 2001. Inelastic constitutive properties and shear localization in Tennessee marble. International Journal for Numerical and Analytical Methods in Geomechanics 25, 109–129.
Jaeger, J.C., Cook, N.G.W., Zimmerman, R., 2007. Fundamentals of Rock Mechanics, fourth ed. Blackwell Publishers, 475 pp.
Lade, P.V., Duncan, J.M., 1975. Elasto-plastic stress–strain theory for cohesionless soil. Journal of the Geotechnical Engineering Division American Society of Civil Engineers 101 (GT10), 1037–1053.
Lin, C.-W., Lee, Y.-L., Huang, M.-L., Lai, W.-C., Yuan, B.-D., Huang, C.-Y., 2003. Characteristics of surface ruptures associated with the Chi-Chi earthquake of September 21, 1999. Engineering Geology 71, 13–30.
Mandel, J., 1966. Conditions de stabilté et postulat de Drucker. In: Kravtchenko, J., Sirieys, P.M. (Eds.), Rheology and Soil Mechanics. Springer Verlag, pp. 58–68.
Matsuoka, H., Nakai, T., 1974. Stress–deformation and strength characteristics of soil under three different principal stresses. Proceedings of Japan Society of Civil Engineers 232, 59–70.
McGarr, A., Gay, N.C., 1978. State of stress in the earth's crust. Annual Review of Earth and Planetary Sciences 6, 405–436.
Mogi, K., 1967. Effect of the intermediate principal stress on rock failure. Journal of Geophysical Research 72, 5117–5131.
Mogi, K., 1971. Fracture and flow of rocks under high triaxial compression. Journal of Geophysical Research 76, 1255–1269.
Murrell, S.A.F., 1963. A criterion for brittle fracture of rocks and concrete under triaxial stress, and the effect of pore pressure on the criterion. In: Fairhurst, C. (Ed.), Proceedings of the Fifth Symposium on Rock Mechanics. Pergamon Press, pp. 563–577.
Nadai, A., 1950. Theory of Flow and Fracture of Solids, vol. 1. McGraw-Hill, New York.
Oku, H., Haimson, B., Song, S.R., 2007. True triaxial strength and deformability of the siltstone overlying the Chelungpu fault (Chi-Chi earthquake), Taiwan. Geophysical Research Letters 34, L09306. doi:10.1029/2007GL029601.
Ottosen, N.S., Runesson, K., 1991. Properties of discontinuous bifurcation solutions in elasto-plasticity. International Journal of Solids and Structures 27, 401–421.
Perrin, G., Leblond, J.B., 1993. Rudnicki and Rice's analysis of strain localization revisited. Journal of Applied Mechanics 60, 842–846.
Rice, J.R., 1976. The localization of plastic deformation. In: Koiter, W.T. (Ed.), Theoretical and Applied Mechanics, Proceedings of the 14th International Congress on Theoretical and Applied Mechanics. North-Holland Publishing Company, Delft, The Netherlands, pp. 207–220.
Rudnicki, J.W., 2004. Shear and compaction band formation on an elliptic yield cap. Journal of Geophysical Research 109. doi:10.1029/2003JB002633.
Rudnicki, J.W., Olsson W.A., 1998. Reexamination of fault angles predicted by shear localization theory. In: Proceedings of Third North American Rock Mechanics Symposium (NARMS'98), Rock Mechanics in Mining, Petroleum and Civil Works, 3–5 June, 1998, Cancun, Mexico. Extended Abstract in International Journal of Rock Mechanics and Mining Sciences 35(415), 512–513.
Rudnicki, J.W., Rice, J.R., 1975. Conditions for the localization of deformation in pressure-sensitive dilatant materials. Journal of the Mechanics and Physics of Solids 23, 371–394.
Rudnicki, J.W., 2008a. Localized failure in brittle rock. In: Shao, J.F., Burlion, N. (Eds.), Thermo-Hydromechanical and Chemical Coupling in Geomaterials and Applications, Proceedings of Third International Symposium GeoProc'2008. Wiley, pp. 25–40.
Rudnicki, J.W., 2008b. Failure of Brittle Rock in the Laboratory and in the Earth, To Appear in Proceedings of XXII International Congress on Theoretical and Applied Mechanics, Adelaide, Australia, 24–30 August.
Shin, T.-C., Teng, T.-L., 2001. An overview of the 1999 Chi-Chi, Taiwan, earthquake. Bulletin of the Seismological Society of America 91, 895–913.
Thomas, T.Y., 1961. Plastic Flow and Fracture in Solids. Academic Press.
Von Kármán, T., 1911. Festigkeitsversuche Unter all Seitigem Druck. Z. Verin Deut., Ingr. 55, 1749–1759.
Wiebols, G.A., Cook, N.G.W., 1968. An energy criterion for the strength of rock in polyaxial compression. International Journal of Rock Mechanics and Mining Sciences 5, 529–549.